Int. J. Electrochem. Sci., 11 **(2016)** 8204 – 8220, doi: 10.20964/2016.10.17

International Journal of ELECTROCHEMICAL SCIENCE
www.electrochemsci.org

Physical & Electrochemical Properties of Green Synthesized Bunsenite NiO Nanoparticles via *Callistemon Viminalis'* Extracts

B.T. Sone[1,2], *X.G. Fuku*[1,2], *M.Maaza*[1,2,*]

[1]UNESCO-UNISA Africa Chair in Nanosciences/Nanotechnology, College of Graduate Studies, University of South Africa, Muckleneuk ridge, P.O. Box 392, Pretoria, South Africa.
[2]Nanosciences African Network (NANOAFNET)-Materials Research Department, iThemba LABS-National Research Foundation, P.O. Box 722, Somerset West 7129, Western Cape Province, South Africa.
[*]E-mail: sonebert@tlabs.ac.za, sonebert@gmail.com, maaza@tlabs.ac.za

Received: 28 January 2016 / *Accepted:* 18 July 2016 / *Published:* 6 September 2016

P-type Bunsenite NiO powders with an average crystallite size of 21 nm (as shown by x-ray diffraction analysis) were produced via biosynthesis and heat treatment using aqueous extracts from red flowers of the plant, *Callistemon viminalis*. SEM showed that the NiO powders consisted of particles with sizes in the 20-35 nm range while XPS confirmed the formation of highly pure NiO. From Raman spectroscopy, strong 1 phonon vibrations at 507.4 cm^{-1} and the existence of a broadened 2-phonon band of reduced intensity at 1096 cm^{-1}confirmed that biosynthesized NiO powders were not only defect-rich/ rich in surface effects but were also nanosized with dimensions less than 100 nm. Through UV-Vis-NIR spectroscopy, the optical band gap for an annealed spin-coated thin film of NiO obtained using the green coloured Ni^{2+}-containing extract of *Callistemon viminalis*, was calculated to be 3.35 eV. A cyclic voltammetric study of the NiO nanopowders on Ni showed the redox processes to be quasi-reversible with the films showing potential for pseudocapacitance and the specific capacitance of the NiO thin films on Ni being estimated at 101 F/g. Electrochemical impedance spectroscopy showed the associated redox processes to be primarily diffusion controlled at room temperature. Through these findings the use of natural plant extracts is hereby shown to be a cost-effective and environmentally friendly alternative to preparing Nickel oxide nanosized powders that can be of use in a variety of energy storage applications.

Keywords: Green synthesis, NiO nanoparticles, Raman spectroscopy, Electrochemical Impedance Spectroscopy, Pseudocapacitance.

1. INTRODUCTION

NiO, a wide band gap (3.7 – 4.0 eV), intrinsic p-type semiconductor metal oxide has been widely investigated for its application in energy storage devices such as Li ion batteries, supercapacitors [1-2], anode material in electrochromic devices and supercapacitors [3,4], water remediation through photocatalysis [5], catalysis of chemical processes [6], and electrochemical sensing [7-8]. With a density of 6.67g/cm^3, a melting point of 1900 °C, NiO adopts the rocksalt NaCl structure, with octahedral Ni(II) and O^{2-} sites. Like many other binary metal oxides, the Ni/O content often deviates from the 1:1 ratio to yield black-coloured non-stoichiometric NiO as opposed to the green-coloured stoichiometric form. NiO is known to have a high work function, its effective hole-transport properties and electron-blocking characteristics, and good thermal stability [9]. With regards to its magnetic ordering pure NiO is antiferromagnetic exhibiting a Neel temperature, T_N of 523 K, below which magnetic ordering is accompanied by a slight rhombohedral distortion.

Numerous methods have been used to prepare NiO thin films and powders , some of which are; electrostatic spray deposition [10], electrospinning [2], hydrothermal synthesis [11], combustion synthesis [12], sputtering of Ni thin films on Ni substrates and subsequent annealing at 400 °C [9], galvanostatic anodization of Ni substrates [4], dip-coating using the SILAR method [13]. Like with other metal oxides, a variety of synthetic processes and techniques as mentioned above are been used to prepare useful forms of NiO, some of which involve the use and release into the environment of harmful reagents and by-products, others which require expensive high vacuum technology and energy intensive processes. An alternative process to the aforementioned cost-intensive and environmentally unfriendly processes and techniques is the synthesis of metal oxides using plant extracts as effective biosynthesis agents [14-17]. These green methods of synthesis allow for an easy, rapid and more environmentally friendly synthesis of several desired oxides [17-24].

In this light and within this contribution, we report for the first time the synthesis of NiO nanoparticles using aqueous extracts from red flowers of the plant, *Callistemon viminalis*. The method used involved no use of solvents and chemicals except for the Ni nitrate precursor employed. Structural and optical characterization of the NiO powder and thin film obtained after annealing confirmed the synthesis of pure p-type NiO nanoparticles. Cyclic voltammetric and EIS studies showed that the nanostructured NiO powder shows potential for applications in batteries and supercapacitors.

2. MATERIALS & METHODS

2.1 Biosynthesis process via Callistemon viminalis aqueous extract

Callistemon viminalis is a plant originally found in Australia. Various phytochemical studies have been carried out on extracts made from different part of these tree species which are the leaves, stem barks, fruits, seeds as well as the flowers [25]. These studies show that the Callistemon generic species is very rich in flavonoids, saponins, steroids, alkaloids and triterpenoids. A summary of the

isolated active compounds obtained from this red dye extracts can be viewed in a previous paper [17]. For this synthesis, fresh red flowers of *Callistemon viminalis* were collected from the Western Cape site of iThemba LABS, South Africa. In a typical setup ~ 7 g of the bottle-brush shaped red flowers were heated in 250 ml of de-ionized water at a temperature between 75-85 °C for 2-3 h yielding a red coloured extract of pH = 3. 75. To 60 ml of the filtered red aqueous extract obtained after cooling to room temperature, was added 10.2 g of $Ni(NO_3)_2.6H_2O$ salt. At room temperature, while swirling, the Ni(II) salt was observed to dissolve completely in the aqueous extract under 3 mins, bringing about a change in colour of the solution from red to dark green. The resultant solution was allowed to settle over a period of 1-2h after which a dark grey precipitate was observed. The precipitate was then separated from the aqueous extract, first by decanting then by centrifuging at 3500 rpm two-three times over successive additions of de-ionized water - this to wash out any residual aqueous extract. The resultant precipitate obtained after decanting the precipitate/H_2O separation was then dried at 250 °C then heated in air at 500 °C for 2h.

2.2. Structural and Optical Characterization

An OXFORD High Resoultion SEM was used to investigate the morphology of the bio-synthesized NiO powders. Elemental analysis obtained through Energy Dispersive X-ray Spectroscopy (EDS) (Figure 2) was carried out using an Oxford Instruments X-Max solid state silicon drift detector (20 keV) coupled to the Oxford HRSEM. For optical characterization absorption/transmittance spectra were measured using a Perkin-Elmer UV-Vis-NIR spectrophotometer in the 200 – 1100 nm range.

To identify the crystallographic phase of the suspected NiO nanoparticles, room temperature XRD analysis was carried out using a Bruker Advanced D8 diffractometer with monochromated Cu Kα radiation of wavelength 1.5406 Å operating at a current of 40 mA and a voltage of 40 kV in the Bragg-Brentano geometry.

To determine the vibrational phonon modes for the NiO nanopowders a Raman spectrum was obtained on a at room temperature using a 514.5 nm excitation line of an Ar^+ laser source in the spectral range of 300-700 nm.

For determining the chemical bonds existing in the annealed NiO powders Fourier-transform-Infrared spectroscopy was carried out in the 400-4000 cm^{-1}range using a Perkin-Elmer spectrometer.

X-Ray Photoelectron spectroscopy was carried out on an XPS microprobe to determine the oxidation states and chemical environment of elements at the sub-surface of the NiO grains. These investigations were acquired using a constant 50 eV pass energy mode, in 0.1 eV increments at 50 ms dwell time with the signal averaged for at hundreds of regular scans. The XPS system was equipped with a dual Mg Kα-Al Kα anode for photoexcitation.

2.3. Electrochemical Characterization

For electrochemical characterization the techniques of Cyclic voltammetry (CV) and Electrochemical Impedance Spectroscopy (EIS) were used. The electrochemical setup used was a

three-electrode system comprising Ni/NiO sheet as working electrode, a Pt-rod as counter electrode, a Ag/AgCl electrode as reference electrode and 2M KOH solution as the electrolyte. The Ni substrate (1cm x 3cm) employed as working electrode had half of its surface sandblasted to create a roughened area that allowed for improved adhesion between the Ni substrate and the NiO nanopowders. To ~ 0.2g of the NiO nanopowders was added 3 ml of distilled water after which ultrasonication was carried out for ~3 min giving rise to a slurry of NiO paste which was drop coated on the cleaned Ni substrates in aliquots of 0.5 ml. After each addition of 0.5 ml of NiO paste the slurry was dried in air in a preheated oven (300 °C) for 2 min giving rise to a well adhered thin film of NiO on Ni. The electrochemical workstation used was a Metrohm potentiostat/galvanostat (PGSTAT302N). Electrochemical impedance spectroscopy was carried out by applying as perturbation a sinusoidal voltage of 5 mV in the frequency range of 100 kHz - 10 mHz at open circuit potential. All measurements were carried out at room temperature.

3. RESULTS AND DISCUSSION

3.1. Surface morphology and elemental analysis

Figure 1 reports the Scanning Electron Microscopy (SEM) micrographs of the NiO powder following annealing at 500 °C of the greyish-brown precipitate. From these it can be established that the nanoparticles are generally spherical in shape, with some degree of aggregation taking place. In spite of some degree of agglomeration observed in the SEM the average particle size distribution can be estimated to lie within 20 – 40 nm range.

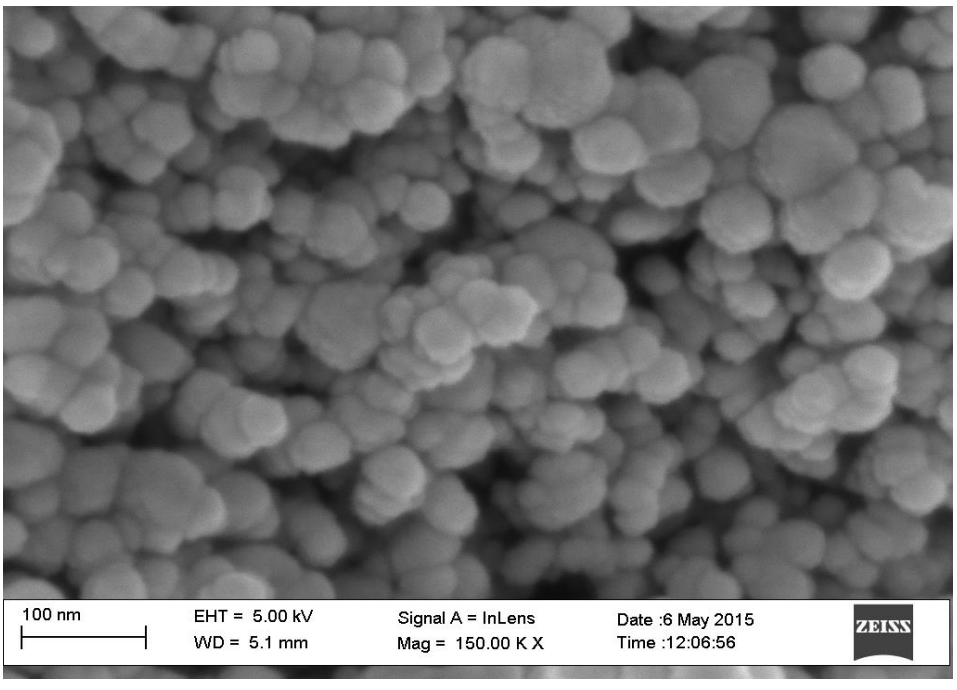

Figure 1. SEM micrograph of NiO nanopowders obtained after annealing at 500 °C for 2h

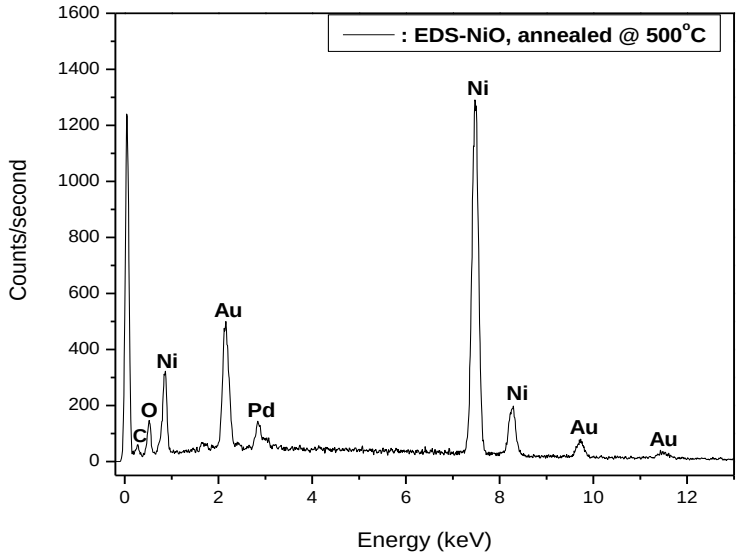

Figure 2. Elemental analysis of NiO nanopowders by Electron Dispersive X-ray Spectroscopy.

EDS spectrum (Figure 2) confirmed the presence of Ni and Oxygen in the annealed powders. The observed peaks of Pd and Au can be attributed to the Au-Pd coating sputtered unto the NiO powders for the purpose of minimizing charging effects. The peaks due to carbon emanate from the carbon tape used as a support for the NiO nanoparticles.

3.2. Crystallographic structure & phase identification

Figure 3 reports a typical XRD profile obtained on the green NiO powder following the annealing at 500 °C of the initially black coloured precipitate obtained after drying in air at 300 °C.

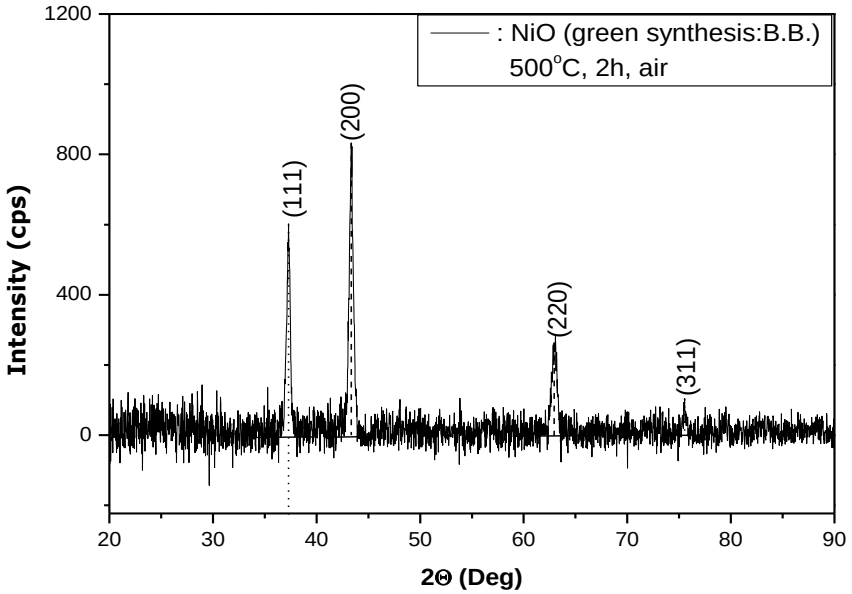

Figure 3. X-ray diffractogram of NiO nanopowders post annealing at 500 °C, for 2h.

Table 1. XRD analysis of crystallite particle size as a function of relevant NiO peaks.

Miller Indices	2θ degrees	Θ(Radians)	FWHM (radians)	Average size <Φ>(nm)	$<d_{hkl}>$(Å)
(1,1,1)	37.3065	0.3256	0.007187	22.6235	2.4057
(2,0,0)	43.3409	0.3782	0.007435	22.2965	2.0859
(2,2,0)	62.954	0.5494	0.010468	17.2557	1.4753
(3,1,1)	75.5231	0.6591	0.009217	21.1426	1.2578

The profile shows a series of intense peaks corresponding to reflections from the (111), (200), (220) and (311) planes which occur angular positions of ~ 37.31, 43.34, 62.95 and 75.52° respectively as indexed to JCPDS card 47-1049. This phase corresponds to the presence of stoichiometric and pure Bunsenite NiO. This rocksalt type structure consists of face-centred cubic (fcc) lattices of oxide anions sitting in tetrahedral site and Ni^{2+} sitting in the octahedral sites. This fcc lattice which belongs to the space group Fm3m (225) has unit cell lattice parameters $<a_{bulk}> = <b_{bulk}> = <c_{bulk}> = 4.177$ Å.

The semi-broad nature of these peaks at their base suggests the nano-scaled nature of the NiO particles. Evidence of this can be seen in the average crystallite size estimate of ~ 21 nm (Table 1) which was calculated using the classical Debye-Scherrer approximation. From the XRD profile it is clear that no pure Ni or $Ni(OH)_2$ was found in the powders after annealing at 500 °C.

3.3. Chemical bonding and vibration spectroscopy

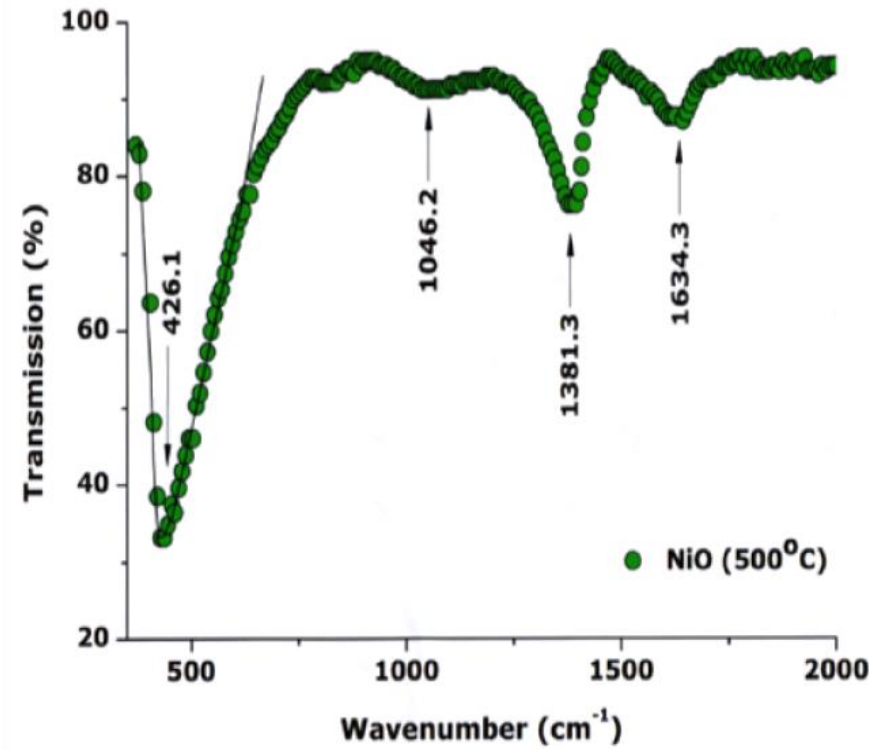

Figure 4. ATR-FTIR spectrum depicting IR vibrational modes in NiO nanopowder by green synthesis.

To confirm again that the prepared powder is NiO and to detect any additional surface/interface bound compounds, Attenuated Total Reflection-FT-IR spectroscopy (Figure 4) was carried out in the 400-2000 cm^{-1} range on the annealed nanopowder at room temperature. The vibrational modes observed at 426 and 1046 cm^{-1} are typical of metal oxide single bonds in the bending mode. The strong absorption band at 426 cm^{-1} is attributed to Ni-O bonds in the bending mode. The broad band of low intensity at 1046 cm^{-1} can be attributed to surface Ni-O stretching vibrations while the weak band at 1634.3 cm^{-1} may well be attributed to O-H vibrations in the bending mode. This along with the strong absorption band at 1381.3 cm^{-1} is reported to emanate from moisture adsorbed at the surface of the NiO powders [26].

As a complimentary study to the ATR-FTIR investigation above, Raman spectroscopy was carried out. Generally, Raman scattering by bulk NiO shows contributions from one phonon transverse-optical and longitudinal-optical modes (TO and LO modes) and two-phonon excitations as well as one, two and four magnon excitations.

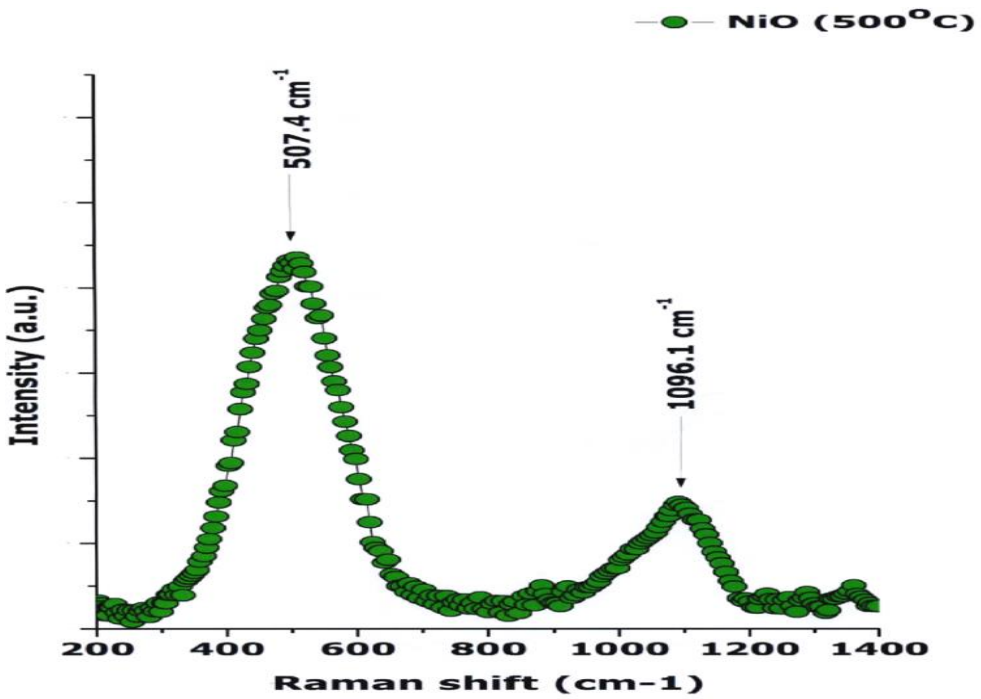

Figure 5. Raman spectrum of NiO nanopowders depicting one-phonon and two-phonon excitations.

If the NiO is defect-rich or anti-ferromagnetically ordered then the contribution of one phonon scattering increases significantly. One phonon TO and LO modes are generally observed to occur at ~ 500-570 cm^{-1}, two phonon 2TO modes at about 700 cm^{-1} , 2 phonon TO + LO modes at ~ 906 cm^{-1}, 2 phonon 2LO modes at ~ 1090 cm^{-1} and 2 magnon scattering at ~ 1550 cm^{-1}. From the Raman spectrum of the NiO nanopowders (Figure 5) prepared through green synthesis, one can distinguish one intense peak centred at about 507.4 cm^{-1} that can be ascribed to one-phonon TO and LO modes. A relatively less intense yet broad peak at 1096.1 cm^{-1} corresponds to vibrations in two phonon 2LO modes [27-28]. The high intensity of the 1 phonon vibration at 507.4 cm suggests that NiO

nanopowder is defect-rich or rich in surface effects. This in agreement with Mironova-Ulmane et al [27] who pointed out that the one phonon band becomes more pronounced in powders while the 2-phonon bands become broadened with that at ~ 906 cm^{-1} practically disappearing. This can be observed in the Raman spectrum of the NiO nanopowder reported in this contribution. Further proof of the nanosized nature of our synthesized NiO powder with average crystallite size being 21 nm is the absence at room temperature of the 2 magnon band (at ~ 1550 cm^{-1}) which is known to dramatically decrease in intensity in nanopowders, becoming undetectable for 100 nm NiO crystallites. This drastic decrease in intensity of the two magnon band in NiO nanopowders with crystallite size less than or equal to 100 nm is attributed to a decrease of antiferromagnetic spin correlations between individual Ni^{2+} ions [29].

3.4. Chemical Valence states by X-Ray Photoelectron Spectroscopy

To further confirm the chemical nature of the NiO nanopowders, X-ray Photoelectron Spectroscopy (Figure 6) was carried out. The initial calibration of the instrument was conducted with a binding energy (B.E.) of 284.5 eV for a C 1s electron. As shown in Figure 6, high resolution energy scans on the NiO nanopowder gives two characteristic main line peaks at BE 855.4 and 873.4eV which correspond respectively to Ni 2p3/2 and Ni 2p1/2 valence states of NiO. The main Ni 2p3/2 and its satellite peak at ~ 860 eV point to the existence of Ni^{2+} ions.

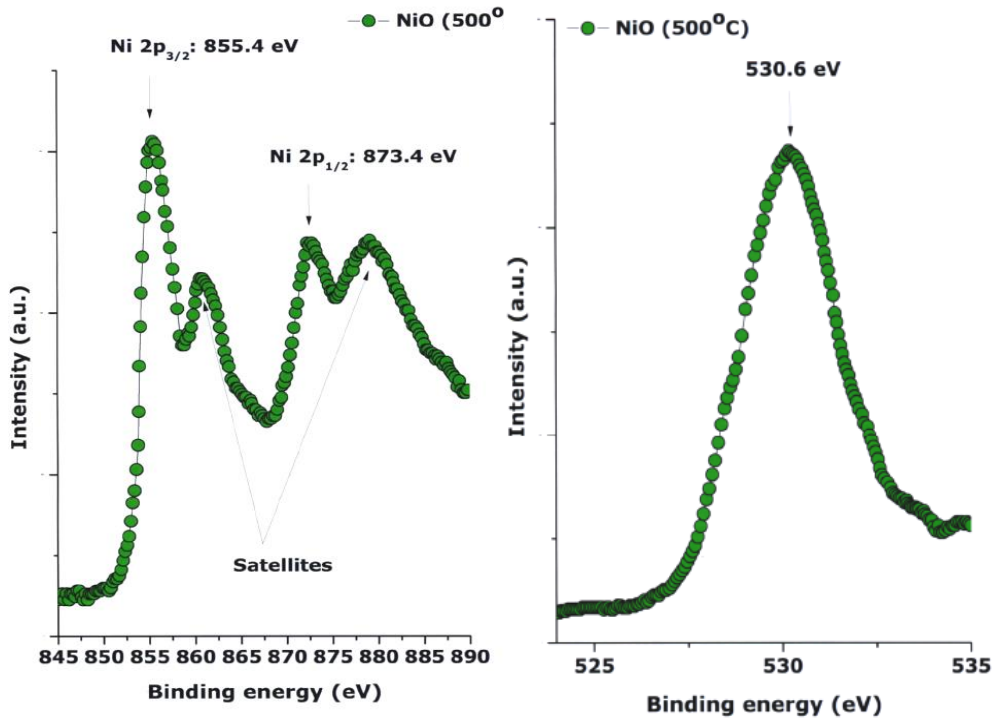

Figure 6. XPS spectra of (a) Ni 2p and (b) O1s core levels of NiO nanopowders prepared using an aqueous extract of *Callistemon viminalis* flowers.

The Ni 2p1/2 peak at 873.4 eV and its satellite peak at ~ 875 eV is ascribed to the Ni^{3+} state which only refers to a species consisting of Ni^{2+} ions with holes and does not imply the existence of the Ni_2O_3 phase in the NiO nanopowder. The O1s peak at a B.E of 530.6 eV can be ascribed to O anions in the NiO nanoparticles and is in agreement with reported data [30]. The broadness of the O1s peaks (527.5 eV – 535 eV) suggests that the peak can be deconvoluted into 3 peaks centred at ~529.5, ~531.1 eV and ~532.8 eV as recently reported [31]. These deconvoluted peaks can respectively be assigned to lattice oxygen (O^{2-}), surface adsorbed oxygen ions (O^-) in oxygen deficient regions (oxygen in the vicinity of Ni vacancies), and an O hydroxyl species or loosely bound oxygen from H_2O absorbed on the NiO surfaces. The observed XPS profile strongly suggests the absence of impurities or hydroxides within the synthesized nanoparticles of Bunsenite NiO.

3.5. Optical Band gap calculation using UV-VIS-NIR

To determine the optical band gap of NiO obtained through green synthesis a total of ~ 8 ml of the green-coloured aqueous extract of *Callistemon viminalis* containing Ni^{2+}, was spin coated unto cleaned glass substrates at 3500 rpm for each addition of 2 ml to the substrate.

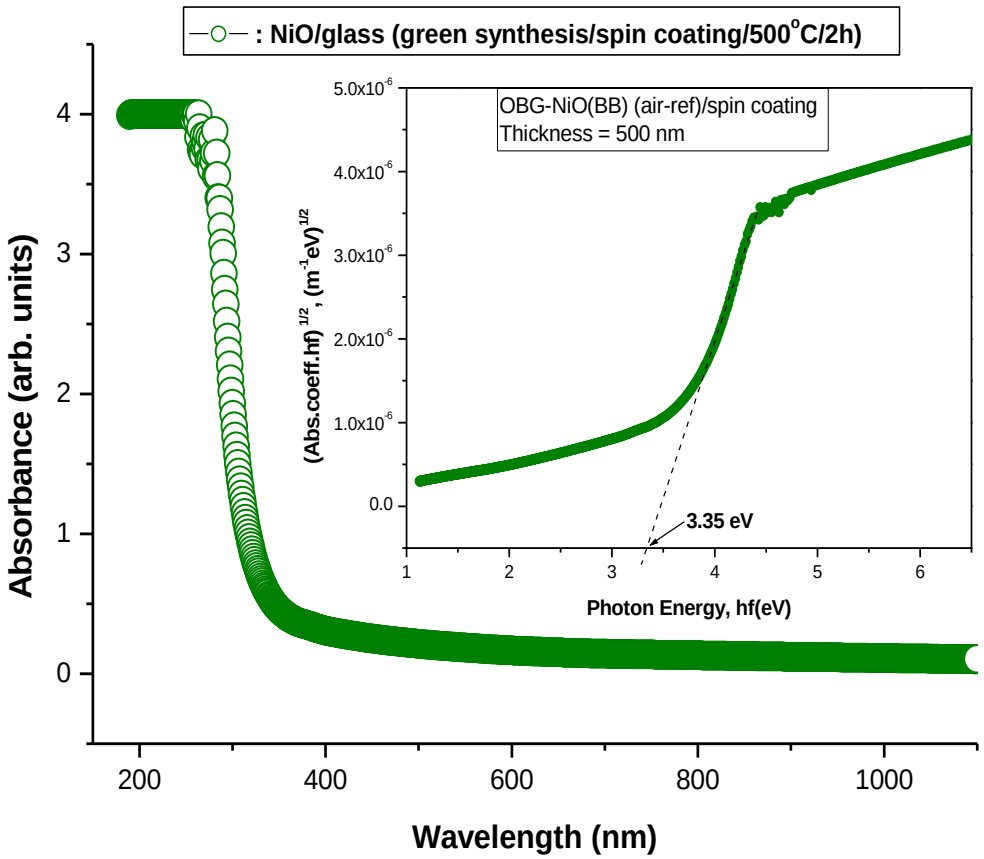

Figure 7. Absorbance spectrum of NiO depicting onset of absorption in UV region (inset shows optical band gap) for spin coated NiO thin film spin annealed at 350 °C.

The obtained thin film on glass was then annealed at 350 °C for 4h. From the absorption profile observed in Figure 7 it can be observed that the onset of absorption in NiO thin film occurs in the UV region. Using Tauc's relation for which $\alpha = (1/d)\ \ln\ (1/T(\lambda))$, with α as the absorption coefficient, *d* is the thickness of the film and *T*(λ)is the wavelength dependent transmittance, the absorption coefficient which is a function of the incident photon energy on the thin film can be used to obtain a close approximation of the optical band gap. Using the standard relationship $(\alpha h\nu)^n = B\ (h\nu - E_g)$ where Eg is the optical band gap, hv is the photon energy, n is 2 for direct band gap transitions or ½ for indirect transitions, and B is constant related to the material, E_g can be calculated by plotting$(\alpha h\nu)^n$ versus the photon energy hv. An extrapolation of the linear part of the plot observed in the high-absorption region gives the energy value of the optical band gap which was calculated for this spin-coated NiO thin film to be 3.35 eV, a value in close agreement with the value of 3.37 eV reported in the literature for NiO films annealed at 350 °C [32].

3.6. Electrochemical properties of bio-synthesized NiO nanoparticles

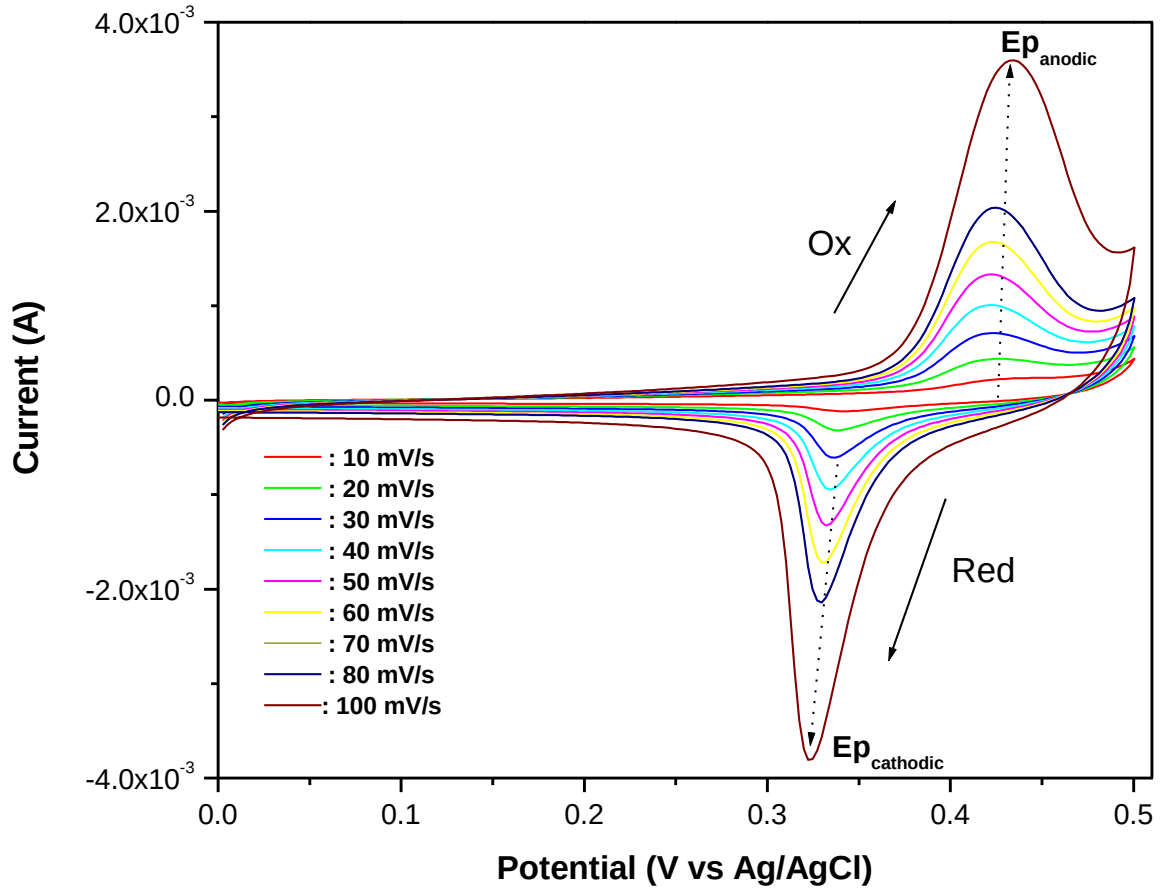

Figure 8. Cyclic Voltammogram of NiO thin film on Ni sheets carried out in 2M KOH, at scan rates 10 - 100 mV/s.

Cyclic voltammetry was carried out within the -0.1 – 0.6 V potential window at scan rates ranging from 10 mV/s to 100 mV/s (Figure 8). From this it was observed that increasing the scan rate resulted in a linear increase in both anodic and cathodic peak currents.

The increase in anodic peak current (oxidation of Ni^{2+} to Ni^{3+}) with increase in scan rate is indicative of electrochemical processes that are controlled by diffusion of ionic species. The anodic peak potential was observed to shift to slightly more positive potentials as the scan rate was increased from 10 -100 mV/s while the cathodic peak potentials (reduction of Ni^{3+} to Ni^{2+}) were observed to increase towards less positive potentials (Fig. 9).

The shifts in peak potential suggest a non-reversible system as evidenced by a plot of the anodic and cathodic peak currents at different scan rates (Fig. 9); a slightly sluggish electron transfer kinetics at the electrode interface and thus a non-linear diffusional system. Also, the potential difference (ΔEa,c) between the anodic peak potential (Ep,a) and the cathodic peak potential (Ep,c) calculated as 112 mV (scan rate of 100 mV/s) which is higher than the theoretical value of 59/n mV synonymous with reversible systems, suggests that the NiO/Ni system is quasi-reversible. For a reversible system the peak potential is independent of the scan rate. This is certainly not the case as observed above with this NiO/Ni system (Table 2).

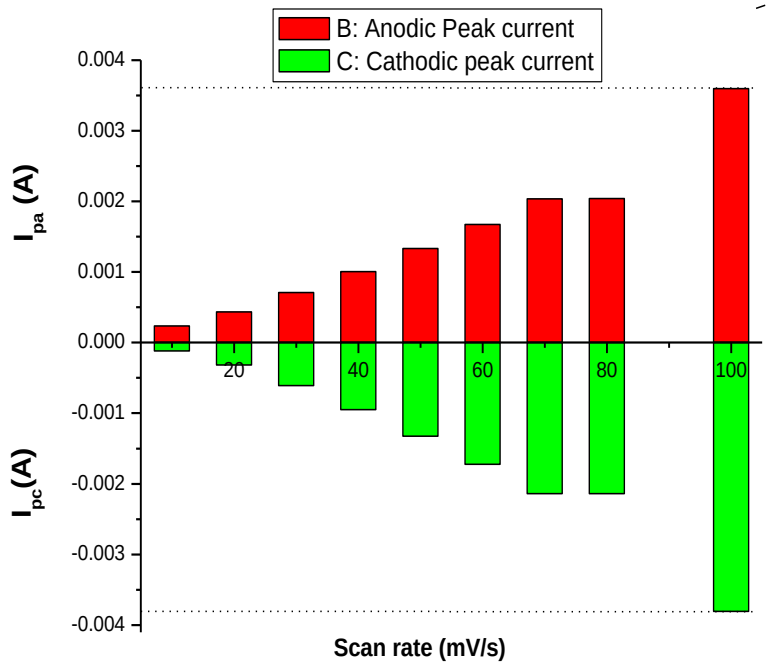

Figure 9. Plot of the anodic and cathodic peak currents at different scan rates.

This may point to the existence of some adsorption and reactions occurring at the electrolyte/electrode interface as the scan rate scales up - possibly the adsorption and reaction of OH- with NiO to form NiOOH as a product of the reaction "$NiO + OH^- \leftrightarrow NiOOH + e^-$ ". The close symmetry of the CV curves and the closeness to unity of the ratio of the peak anodic current to the peak cathodic current at scan rates 50 – 100 mV/s, indicates that the system has some degree of reversibility at higher scan rates. At lower scan rates the NiO/Ni system shows clear irreversibility.

The two distinct redox peaks in the vicinity of 0.32 –0.34 V and 0.43–0.45 V show that the NiO nanopowders exhibit Faradaic pseudo-capacitance with the NiO layer getting its charge from the fast & reversible redox reactions occurring at the electrode-electrolyte interface. That the charge storage capacity of the NiO/Ni system is principally dependent on Faradaic redox processes is also evidenced by the non-rectangular shape of the cyclic voltammetric curves. The transfer and insertion/adsorption of OH^- ions from the electrolyte to the NiO layer is a relative slow process thus rate-limiting when compared to the rapid electronic exchanges occurring between the different NiO-based redox species.

Table 2. Measure of reversibility (I_{pa}/I_{pc}) of NiO/Ni system at scan rates ranging from 10-100 mV/s

Scan rate (mV/s)	10	20	30	40	50	60	70	80	100
Ipa/Ipc	2.00	1.37	1.16	1.06	1.00	0.977	0.953	0.953	0.945

A scatter plot of the anodic peak current, I_{pa},vs the square root of the scan rate (Figure 10a) for scan rates in the 30-100 mV/s range, show that the peak anodic current increases non-linearly with the square root of the scan rate. Non-linearity not withstanding the increase is an indication that the oxidation of the NiO nanopowders is a diffusion-controlled process. A deviation from a straight line (represented by a dashed line) as the scan rates increased from 50 mV/s and beyond is however clearly observed.

(a)

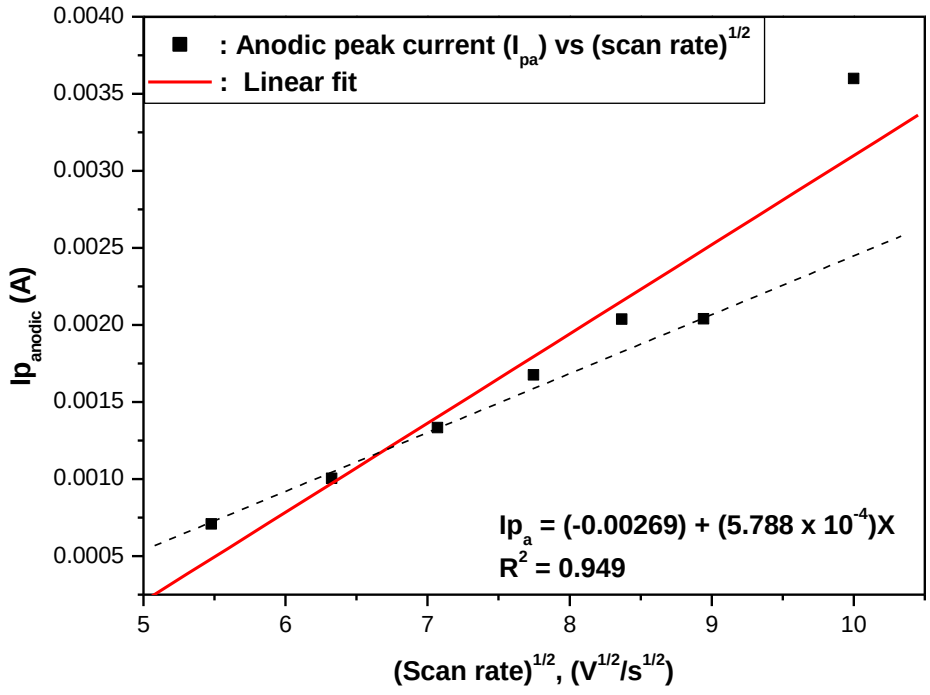

(b)

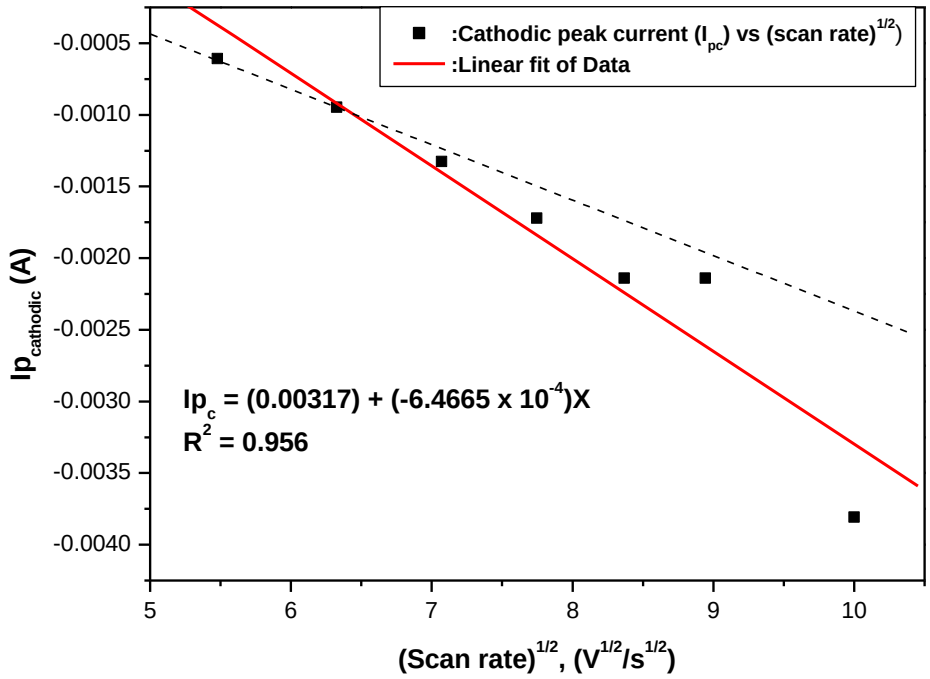

Figure 10. Scatter plot of (a) anodic peak current vs square root of scan rate (b) cathodic peak current vs square root of scan rate. (Red solid line is a linear fit of actual data. Dashed line represents an ideal linear system)

This deviation suggests the occurrence of reactions at the NiO surface such as those involving the adsorption and insertion of species like OH^- ions and H_2O into the NiO thin film. The porosity of the NiO thin film could also lead to a deviation from a straight line plot. A linear fit of the plot which yielded a straight line with regression R^2 = 0.949 suggests that the anodic peak current can be described as being a linear function of the $(\text{scan rate})^{1/2}$. A linear fit with regression of R^2 = 0.956 was obtained for a plot of the cathodic peak current, I_{pc}, vs the square root of the scan rate (Fig. 10b). A similar deviation from a straight line (see dashed line) is observed as from 50 mV/s and can be explained by the porosity of the NiO layer as well as a reverse process of desorption and de-insertion of OH^- ions from the NiO/Ni layer.

From the Nyquist plot (Figure 11) obtained through EIS measurements, it can be observed for the NiO coated Ni substrate the absence of a depressed semi-circle which points to the existence of very little charge transfer resistance of the NiO layer/electrolyte interface to the diffusion and insertion of ionic species from the KOH electrolyte.

This may be accounted for by the morphology of the NiO nanopowders that offer a larger surface area and higher porosity which offer short diffusion pathways and allow for rapid insertion and diffusion of large OH- ions to redox active sites in the NiO electrode film. For the bare Ni substrate, a large depressed semi-circle synonymous with a large charge-transfer resistance, Rct, can be observed. This anomaly for a Ni sheet may be explained by the formation of a thin oxide layer which may have formed during the process of sandblasting. The vertical line inclined at ~ 45° to the real Z-axis in the low frequency region denotes Warburg's impedance and points to the fact that the transport of OH^-

ions to and fro the electrode is diffusion controlled. The steeper the slope of the vertical line the higher the diffusion rate of OH^- ions into the pores. The inset shows an equivalent circuit diagram for the NiO/Ni system in which the solution resitance, R_e, comprises the resistance of the bulk electrolyte and the electrode resistance, C_{dl} is the double layer capacitance, Z_w is the Warburg impedance and the R_{ct} is the Faradaic charge transfer resistance [33].

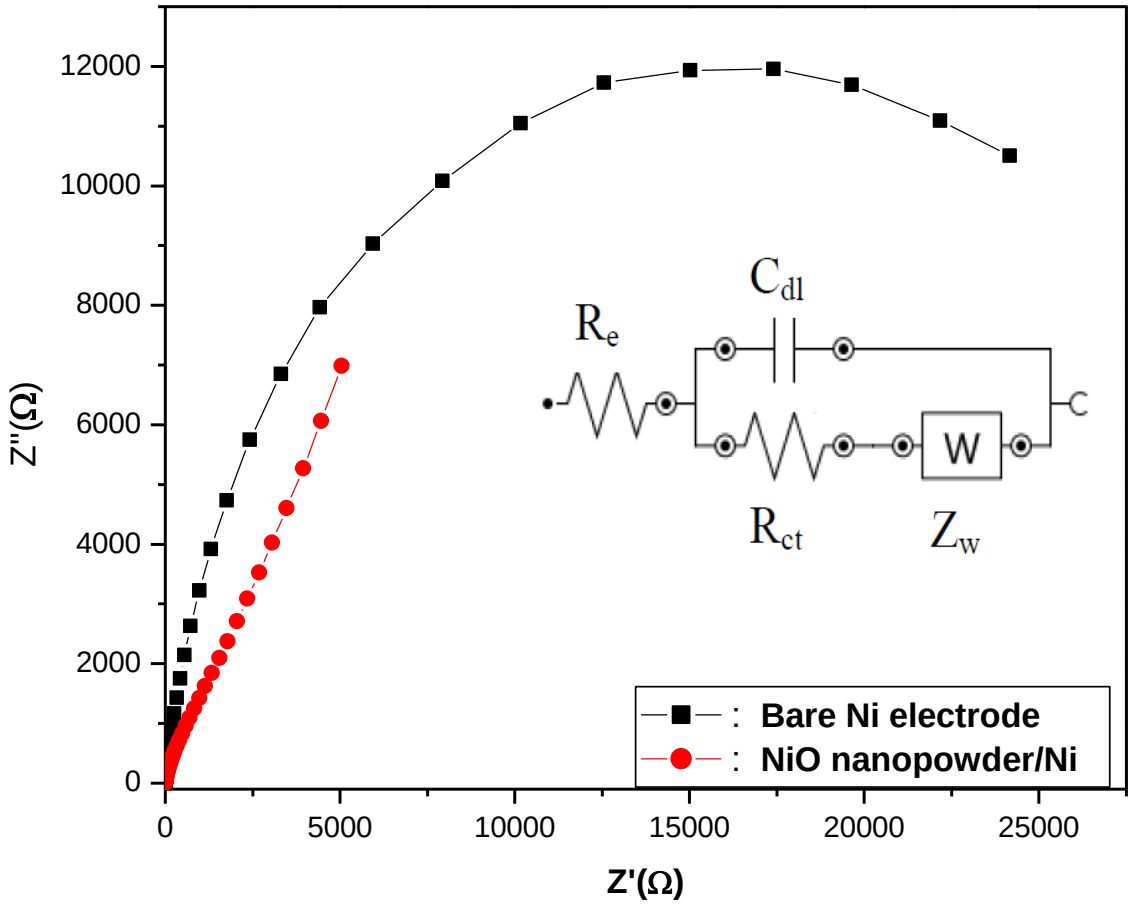

Figure 11. Nyquist plot obtained from EIS measurements in a 2M KOH, for a bare Ni and NiO coated Ni electrode, at 5 mVa.c. perturbations in a 100 kHz-10 mHz range (inset shows the equivalent circuit).

Using the Bode plot (Figure 12) it can be deduced that the resistance of the solution, R_S= 2.71 Ohms and the charge transfer resistance for the NiO thin film on Ni, R_{ct} = 8616.47 Ohms.

This is consistent with the nature of the electrolyte which is an ionic solution with labile K^+, OH^- and that of the metal oxide which should be more semiconducting to insulatory offering a higher resistance to ion insertion and de-insertion.

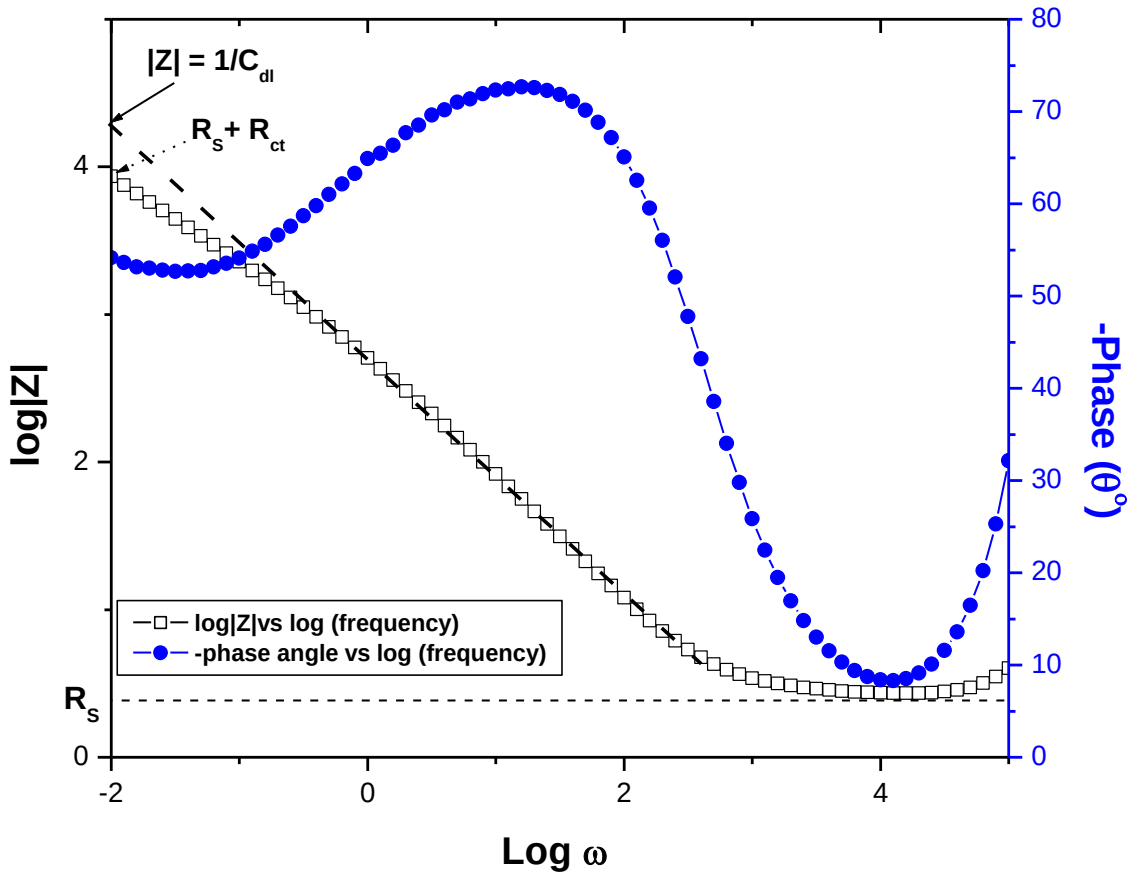

Figure 12. Bode plot obtained from EIS measurements on a NiO/Ni electrode in 2M KOH, using 5 mV a.c. perturbations in a 100 kHz- 10 mHz range.

From the extrapolation of the plot of log|Z| vs log ω to the log|Z| axis, the double layer capacitance, C_{dl}, of the NiO dielectric thin film can be calculated using the relation $|Z| = 1/ C_{dl}$ where |Z| is the absolute impedance. Based on this relation the double layer capacitance = 5.3906 x 10^{-5}F ~ 0.54 μF. From the relation $C_i = q/V_f\text{-}V_i$ and $q = \int_{Vi}^{Vf} I(V)dV/v_{sr}$, where C_i = capacitance, V_f = final potential, V_i = initial potential, q = overall charge at a given scan rate, $\int_{Vi}^{Vf} I(V)dV$ = average current density per unit area and v_{sr} = given scan rate, the charge and capacitance at 100 mV/s was calculated to be 5.686 x 10^{-3} C and 5.0633 x 10^{-2} F respectively. As observed, it can expected that the NiO layer will have a superior capacitance (5.0633 x 10^{-2} F) compared to that of the double-layer (5.3906 x 10^{-5}F) [34]. At m = 0.5 mg (mass of the NiO thin film on Ni) the specific capacitance, $C_s = q/m(V_f\text{-}V_i)$ can thus be estimated as = 101.27 F/g. This value is similar to that in work reported by Basri et al [35]. In theory, the capacitor behaves best when θ ≈ −90◦. However, the phase angle of the NiO/Ni electrode (θ ≈ −75◦) was far below the expected values for capacitors as expected for a semiconductor. The value is however similar to that reported for $Ni(OH)_2$/NiO thin films on steel substrates [36]. Subsequently, the results reveal the relationship between capacitance vs. frequency which indicate that as the frequency increases, capacitance increases showing the potential for pseudocapacitor applications of NiO. These results which are comparable to that reported in the literature show that the

NiO nanopowders prepared by this method of biosynthesis show potential for pseudocapacitor applications.

4. CONCLUSION

We report for the first time the successful synthesis of NiO nanospheres using as an effective biosynthesis agent aqueous extracts from red flowers of the plant, *Callistemon viminalis*. Structural and optical characterization of these powders (annealed at 500 °C), using complementary techniques such as SEM, EDS, XRD, FTIR-ATR, Raman, XPS and UV-Vis-NIR spectrophotometry confirm the formation of pure, crystalline Bunsenite NiO nanospheres with an average particle size of ~ 21 nm. A cyclic voltammetric study of drop-coated thin films of the crystalline NiO nanopowders on Ni showed the redox processes to be quasi-reversible with the films showing good potential for pseudocapacitance and the specific capacitance of the NiO thin films on Ni being estimated at 101 F/g. Electrochemical impedance spectroscopy showed the associated redox processes to be primarily diffusion controlled at room temperature. These results demonstrate that the bio-synthesized NiO nanopowders could be of use in a variety of applications among which is energy storage in pseudocapacitors.

ACKNOWLEGDEMENTS
This research was generously supported by Grant 92541 of the National Research Foundation of South Africa, the French Centre National pour la Recherche Scientifique (CNRS), iThemba LABS, the UNESCO-UNISA Africa Chair in Nanosciences and Nanotechnology, the Abdus Salam International Centre for Theoretical Physics (ICTP) via the Nanosciences African Network as well at the African Laser Centre (ALC), to whom we are all grateful.

References

1. Y. Ma, L. Sheng, H. Zhao, K. Am, L. Yu, J. Xu, X. Zhao, *Solid State Sci*., 44 (2015) 49-55.
2. M. Kundu, L. Liu, *Mater. Lett*., 144 (2015) 114-118.
3. X. Qi, G. Su, G. Bo, L. Cao, W. Liu, *Surf. Coat. Technol*., 272 (2015) 79-85.
4. M. Chiku, M. Toda, E. Higuchi, H. Inoue, *J. Power* , 286 (2015) 193-196.
5. J. Zhao, Y. Tan, K. Su, J. Zhao, C. Yang, L. Sang, H. Lu, J.H. Chen, *Appl. Surf. Sci*., 337 (2015) 111-117.
6. A.L. Gajengi, T. Sasaki, B.M. Bhanage, *Catal.Commun*., 72 (2015) 174-179.
7. M. Tadic, D. Nikolic, Matjaz, G.R. Blake, *J. Alloys Compd*., 647 (2015) 1061-1068.
8. R.A. Soomro, Z.H. Ibupoto, Sirajuddin, M. I. Abro, *Sens. Actuators*, B 209 (2015) 966-974.
9. Y. Zhang, *Appl. Surf. Sci*., 344 (2015) 33-37.
10. B. Ksapabutr, P. Nimmuan, M. Panapoy, *Mater. Lett*., 153 (2015) 24-28.
11. R.A. Soomro, Z.H. Ibupoto, Sirajuddin, M. I. Abro, *Sens. Actuators*, B 209 (2015) 966-974.
12. K. Tao, P. Li, L. Kang, X. Li, Q. Zhou, L. Dong, *J. Power Sources*, 293 (2015) 23-32.
13. Y. Akaltun, T. Cayir, *J. Alloys Compd*., 625 (2015) 144-148.
14. F.T. Thema, E. Manikandan, M.S. Dhlamini, M. Maaza, *Mater. Lett*., 161 (2015) 124-127.
15. N. Thovhogi, A. Diallo, A. Gurib-Fakim, M. Maaza, *J. Alloys Compd.*, 647 (2015) 392-396.
16. A. Diallo, B.D. Ngom, E. Park, M. Maaza, *J. Alloys Compd*., 646 (2015) 425-430.

17. B.T. Sone, E. Manikandan, A. Gurib-Fakim, M. Maaza, *J. Alloys Compd*., 650, (2015) 357-362.
18. F.T. Thema, E. Manikandan, A. Gurib-Fakim, M. Maaza, *J. Alloys Compd*., 657 (2016) 655-661.
19. N. Thovhogi, E. Park, E. Manikandan, M. Maaza, A. Gurib-Fakim,*J. Alloys Compd*., 655 (2016) 314-320.
20. E. Ismail, A. Diallo, M. Khenfouch, S.M. Dhlamini, M. Maaza, *J. Alloys Compd*., 662 (2016) 283-289.
21. N. Thovhogi, A. Diallo, A. Gurib-Fakim, M. Maaza,*J. Alloys Compd*., 647 (2015) 392-396.
22. A. Diallo, B.D. Ngom, E. Park, M. Maaza,*J. Alloys Compd*., 646 (2015) 425-430.
23. B.T. Sone, E. Manikandan, A. Gurib-Fakim, M. Maaza, *Green Chemistry Letters & Reviews*, 9 (2016) 85-90.
24. A. Diallo, A.C. Beye, T.B. Doyle, E. Park & M. Maaza, *Green Chemistry Letters & Reviews*, 8 (2015) 32-36.
25. A. Gurib-Fakim, *Molecular Aspects of Medicine*, 27 (2006)1-93.
26. Z. Qing, L. Haixia, L. Huali, L. Yu, Z. Huayong, L. Tianduo, *Appl. Surf. Sci*., 328 (2015) 525-530.
27. N. Mironova-Ulmane, A. Kuzmin, I. Steins, J. Grabis, I. Sildos and M. Pars, *J. Phys.: Conf. Ser*. 93 (2007) 012039.
28. M. Yao, Z. Hu , Y. Liu, P. Liu, Z. Ai, *J. Alloys Compd*., 648 (2015) 414–418.
29. A.C. Gandhi, C-Y. Huang, C. C. Yang, T. S. Chan, C-Li. Cheng, Y-R.Ma and S.Y. Wu, *Nanoscale Res. Lett.*, 6 (2011) 485 – 498.
30. L. Li, B. Cheng, Y. Wang, J. Yu, *J. Colloid Interface Sci*., 449 (2015) 115-121.
31. L. Cao, D. Wang, R. Wang, *Mater. Lett*., 132 (2014) 357–360.
32. A.Venter, J.R. Botha, S. *Afr J Sci.* 2011;107(1/2), Art.#268, 6 pages.
33. B. Ren, M. Fan, Q. Liu, J. Wang, D. Song, X. Bai, *Electrochim. Acta*, 92 (2013) 197-204.
34. F. I. Dar, K. R. Moonooswamy and M. Es-Souni, *Nanoscale Res. Lett.*, 8 (2013) 363-369.
35. N. H. Basri, M. Deraman, M. Suleman, Najah Syahirah Mohd Nor, Besek N. Mohamad Dolah, M. I. Sahri, S. A. Shamsudin, *Int. J. Electrochem. Sci.*, 11 (2016) 95 – 110.
36. Assumpta C. Nwanya , Solomon U. Offiah, Ifeanyichukwu C. Amaechi, Solomon Agbo, Sabastine C. Ezugwu, B.T. Sone, Rose U. Osuji, Malik Maaza, Fabian I. Ezema, *Electrochimica Acta*, 171 (2015) 128–141.